J Nanopart Res (2013) 15:1532
DOI 10.1007/s11051-013-1532-6

RESEARCH PAPER

A novel method for controlled synthesis of nanosized hematite (α-Fe_2O_3) thin film on liquid–vapor interface

Pawan Kumar · Raj Kumar Singh · Nitin Rawat · Partha Bir Barman · Subhash Chander Katyal · Hwanchol Jang · Heung-No Lee · Rajesh Kumar

Received: 27 June 2012 / Accepted: 22 February 2013 / Published online: 6 March 2013

Abstract Hematite (α-Fe_2O_3) films with a high quality surface morphology have been formed at the liquid–vapor interface using a novel approach. The surface morphology/size of the nanoparticles constituting the film is tuned in a controlled manner. It is observed that the concentration of polyvinyl alcohol in the precursor Fe^{3+}/Fe^{2+} solution, the concentration of ammonia (NH_3) vapor, and the annealing temperature are factors influencing the surface morphology/size of nanoparticles. The diameter of the α-Fe_2O_3 nanoparticles inside the film is controlled to be 2–15 nm by varying the synthesis conditions, and accordingly the films have roughness in the 1.34–6.8 nm range. The prepared α-Fe_2O_3 films are crystalline in nature and exhibit superparamagnetic behavior at room temperature.

Keywords α-Fe_2O_3 nanoparticles · NH_3 vapor · Concentration of PVA · Annealing temperature

P. Kumar · P. B. Barman · R. Kumar
Jaypee University of Information Technology, Waknaghat, Solan 173234, Himachal Pradesh, India

R. K. Singh
CSIR-Indian Institute of Petroleum, Dehradun 248005, India

N. Rawat · H. Jang · H.-N. Lee · R. Kumar (✉)
Gwangju Institute of Science and Technology, Gwangju 500712, Republic of Korea
e-mail: rajesh.kumar@juit.ac.in; rajeshkumarf11@gmail.com

H.-N. Lee
e-mail: heungno@gist.ac.kr

S. C. Katyal
Jaypee Institute of Information Technology, Sector 128, Noida 201304, Uttar Pradesh, India

Introduction

Iron oxides attract interest as materials because of their catalytic, magnetic, and semiconducting properties (Aronniemi et al. 2004; Chandra et al. 2010). The material α-Fe_2O_3, an iron oxide, in particular has been suggested for applications as a catalyst (Liu et al. 2007a, b), a magnetic material (Wu et al. 2006), a photo catalyst (Chirita and Grozescu 2009), an anode in Li-ion batteries (Ryu et al. 2010), in photo electrochemical solar cells (Shinde et al. 2011; Ahmmad et al. 2009), a water splitter (Shen et al. 2012), in nonlinear optics (Zhou et al. 2000), and for gas sensors (Gou et al. 2008; Zhang et al. 2011).

For any technological application, the size of the α-Fe_2O_3 nanoparticles composing a film is an important factor. The small size of α-Fe_2O_3 nanoparticles provides a large surface area for adsorption/desorption of the chemical species in contact with it, thus allowing for good performance of the application device using the film. Most of the properties such as superparamagnetism (Lindgren et al. 2002; Ramachandran and Ramachandra Rao 2007), light absorption (Mulmudi et al. 2011), Li-ion adsorption

(Turkovoć et al. 2011; Jin et al. 2012), optical limiting (Singh et al. 2008), and gas sensing (Aronniemi et al. 2008) depend upon the size of α-Fe_2O_3 nanoparticles. The size of α-Fe_2O_3 nanoparticles depends upon the synthesis methods (Dong et al. 2012) as well. So far, many methods of synthesizing α-Fe_2O_3 films such as chemical vapor deposition (CVD) (Mathur et al. 2006; Ge et al. 2009; Chatzitheodorou et al. 1986), reactive ion beam sputtering (Birkholz et al. 1992), laser-assisted CVD (Sivako et al. 2005), and ultrasonic spray pyrolysis (Cesar et al. 2006; Fu et al. 2003; Jia et al. 2005; Mahapatra et al. 2009; Park et al. 2009; Miller et al. 2004; Zang et al. 2010; Kay et al.2006; Glasscock et al. 2007; Kim et al. 2011) have been reported. Also, a well-known vapor–liquid–solid (VLS) method (Liu et al. 2007a, b; Hwang et al. 2009) has been used to synthesize α-Fe_2O_3 (Kumar et al. 2009). Nevertheless, most of them are not cost effective and lack the flexibility of formation and transformation of the film on a desired substrate.

Methods employing polymers have also been reported (Morishita et al. 2005; Omi et al. 2001; Liu et al. 2007a, b). These methods combine different polymers, utilizing their emulsion forming tendency and the adsorption/encapsulation property of metal oxide nanoparticles into their dispersed polymeric micro and nanospheres. In most of the methods, a polymer such as polyvinyl alcohol (PVA) is frequently used in the synthesis of magnetic nanocomposites as it is a unique, synthetic, nontoxic, biocompatible, water-soluble, and easily available polymer. Also, it has a large number of –OH groups for interaction, which is a strong reason for its utilization.

Here, we present a novel approach for the formation of α-Fe_2O_3 film using PVA polymer in the precursor solution. Initially, a PVA composite film was formed on the liquid–vapor interface, which after transferring over a glass substrate and annealing in a furnace was converted to an α-Fe_2O_3 film. In this work, tuning the size of nanoparticles/surface morphology as well as the flexibility of transferring the film that is formed at the liquid–vapor interface to a desired substrate has been achieved. By changing the synthesis parameters, such as concentration of NH_3 vapor, film annealing temperature, and concentration of PVA, films of different morphologies have been formed. The method presented here is a comparatively low temperature method for the formation of α-Fe_2O_3 film.

Experimental

Material synthesis

In order to make a precursor solution, $FeCl_3 \cdot 6H_2O$ (purity 99.99 %), as a source of Fe^{3+} ions, and $FeCl_2$ (purity 99.99 %), as a source of Fe^{2+} ions, were purchased from Sigma-Aldrich. NH_3 solution (conc. 25 %) was purchased from E. Merck. The host polymer PVA (molecular weight = 125,000) was purchased from S. D. Fine Chemicals Limited, India.

Method

A precursor solution with 24 mM $FeCl_2$ and 22 mM $FeCl_3 \cdot 6H_2O$ was initially prepared. Then, a measured amount, as mentioned in the following discussion, of PVA was added to the precursor solution. The solution was stirred for 10 min at 80 °C and immediately transferred to a petri dish placed in an argon (Ar) chamber as shown in Fig. 1. Then, a measured volume of NH_3 vapor was poured through a syringe into the chamber containing the solution in the petri dish. After pouring NH_3 vapors, the chamber was kept sealed for 10 min to facilitate the chemical reaction between the NH_3 vapor and the PVA-containing precursor at the surface of the solution. Consequently, the liquid–vapor interface converted into a thin floating film. The obtained film was transferred to the surface of distilled water filled in another petri dish. The film was then deliberately transferred to the surface of a glass substrate.

The above experiment was repeated in order to observe the effect of NH_3 vapor concentration on the film morphology. The films were formed by using 4, 6, and 8 % volume of NH_3 in the reaction chamber. Similarly, a second set of films was formed by varying the concentration of PVA in the precursor solution. The PVA concentrations were 16, 32, and 64 μM, while 6 % volume of NH_3 vapor was used inside the chamber. Then, in order to form α-Fe_2O_3 films, the films obtained in the above experiments were annealed at 500 °C for 2 h in an Ar gas environment. We also performed an experiment to study the effect of annealing temperature on surface morphology. For this experiment, the films were formed using 6 % NH_3 vapor and 32 μM PVA. The film was annealed at temperatures of 250 and 500 °C for 2 h in Ar gas environment.

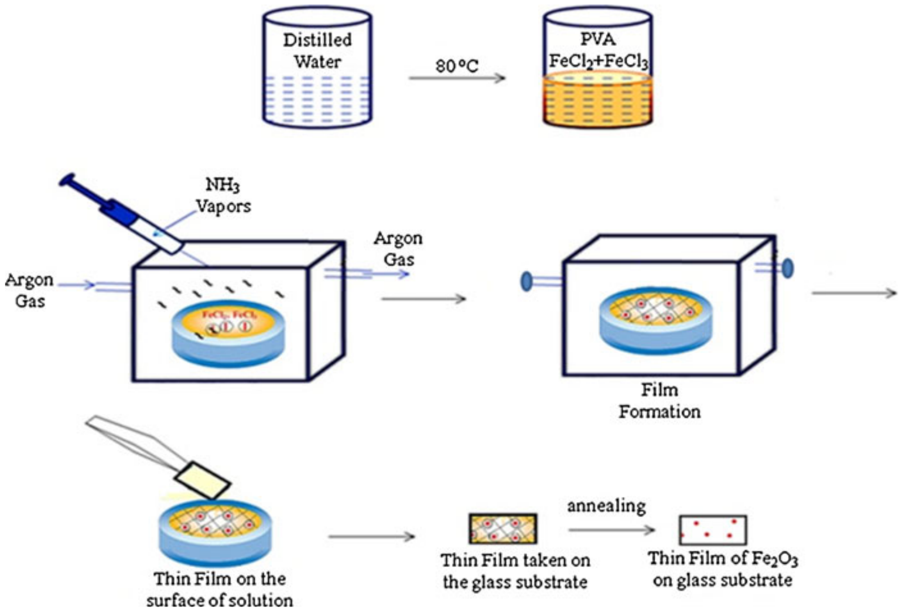

Fig. 1 Schematic illustration of nanosized hematite (α-Fe_2O_3) film formation on a liquid–vapor interface

Microstructural and magnetic characterization

Scanning electron microscopy (SEM), transmission electron microscopy (TEM), energy dispersive X-ray spectroscopy (EDX), atomic force microscopy (AFM), and X-ray diffraction (XRD) techniques have been used for the structural characterization of the films and to study their morphology. Magnetic characterization has been carried out using the vibrating sample magnetometer (VSM) and magnetic property measurement system (MPMS).

Results and discussion

Mechanism of nanosized hematite (α-Fe_2O_3) film formation

In the Fe^{3+}/Fe^{2+}/PVA system, the possible mechanism of the film formation on the liquid–vapor interface is via the encapsulation or adsorption of Fe^{2+}/Fe^{3+} ions on the PVA chain. The bonding between Fe^{2+}/Fe^{3+} and PVA may have occurred due to the interaction of PVA hydroxyl groups with the hexaaquairon complex species because it is well known that chloride salts of Fe^{2+} and Fe^{3+} form

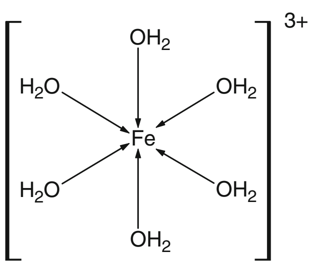

Fig. 2 Structure of $[Fe(H_2O)_6]^{3+}$ complex formed by Fe^{3+} in aqueous solution

octahedral hexaaquairon complexes in water. One of the complexes of Fe^{3+} is shown in Fig. 2.

Here, each of the six water molecules is attached to the central Fe^{3+} ion via a coordinate bond using one of the lone pairs on the oxygen. The hydrogen atoms attached to the water ligands are sufficiently positive and they can be pulled off in a reaction involving water molecules in the solution. Here, the water molecule works as a weak base.

$$\left[Fe(H_2O)_6\right]^{3+} + H_2O \ \rightarrow \ \left[Fe(H_2O)_5OH\right]^{2+} + H_3O^{+} \quad (1)$$

Further, loss of hydrogen ions may take place from a second and a third water molecule, resulting in the final neutral insoluble form, i.e., $[Fe(H_2O)_3OH_3]$.

$$\left[\mathrm{Fe(H_2O)_6}\right]^{3+} + n\mathrm{H_2O} \rightarrow \left[\mathrm{Fe(H_2O)_{6-n}OH_n}\right]^{3-n+} + n\mathrm{H_3O^+} \quad (2)$$

Fe^{2+} also forms a similar type of water coordinated species. The added PVA can form a hydrogen bond between the –OH groups present in its chains and these aqua iron complex species. If the hydroxyl groups from the different PVA chains take part in hydrogen bonding, then it may also lead to PVA cross-linking (Lin et al. 2003). So, using this mechanism, the Fe^{2+}/Fe^{3+} ions in the solution may be encapsulated in the polymer chain. When the NH_3 vapor is poured into the reaction chamber, these adsorbed or encapsulated Fe^{2+}/Fe^{3+} ions get converted into the nanoparticles of Fe_3O_4, in accordance with the following reaction:

$$2\mathrm{FeCl_3} + \mathrm{FeCl_2} + 8\mathrm{NH_4OH} \rightarrow \mathrm{Fe_3O_4} + 8\mathrm{NH_4Cl} + 4\mathrm{H_2O} \quad (3)$$

Due to the increased pH value of the solution, co-precipitation of Fe_3O_4 takes place through substantial PVA cross-linking and solidification, resulting in the formation of a thin film over the surface of the solution. If a higher concentration of NH_3 is available, the reaction on the surface will be faster and it will lead to the formation of a thick film. Moreover, a higher concentration of the NH_3 vapor will cause diffusion to the solution beneath the surface layer so that a further thicker film with agglomerated nanoparticles will form. When the (Fe_3O_4)/PVA nanocomposite film is annealed after transferring onto a glass substrate, the organic PVA matrices evaporate and Fe_3O_4 oxidizes to form α-Fe_2O_3. Hence, after annealing, the glass substrate remains coated with a film of α-Fe_2O_3 nanoparticles.

$$4\mathrm{Fe_3O_4} + \mathrm{O_2} \rightarrow 6\mathrm{Fe_2O_3} \quad (4)$$

Simultaneously, the formation of α-Fe_2O_3 may also take place according to the following reaction:

$$2\mathrm{FeCl_3} + 6\mathrm{NH_4OH} \rightarrow \mathrm{Fe_2O_3} + 6\mathrm{NH_4Cl} + 3\mathrm{H_2O} \quad (5)$$

Effect of NH_3 concentration

The precursor solution was exposed successively to three concentrations viz. 4, 6, and 8 % of NH_3 vapors. Then, the obtained films after their transfer to the glass substrate were annealed for 2 h at 500 °C in a horizontal tube furnace in an Ar gas environment. SEM images of the annealed films are shown in Fig. 3. In the SEM images, a slight variation in the size of the particles with the increase in concentration of the NH_3

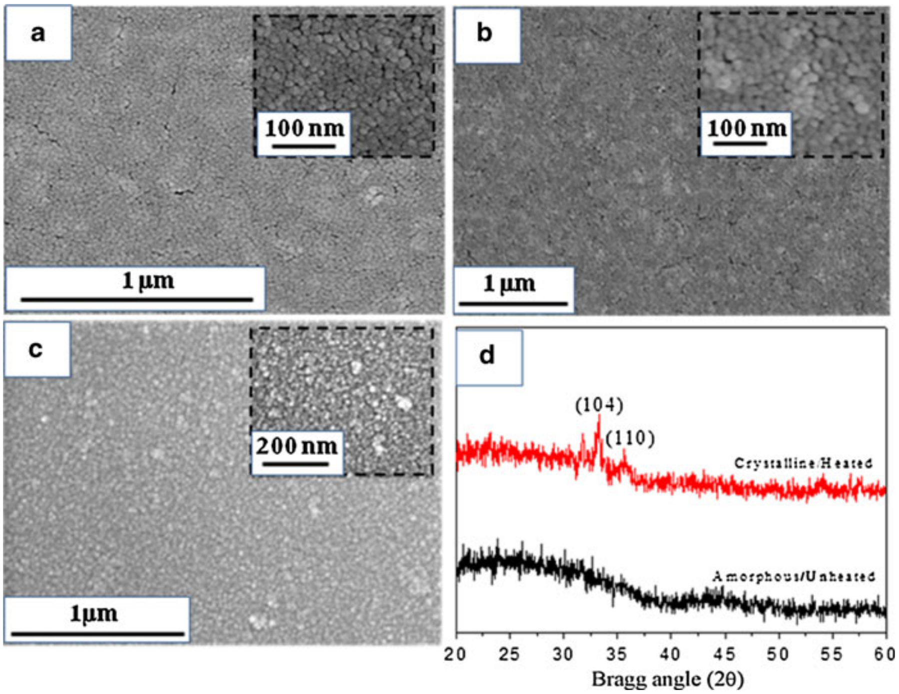

Fig. 3 SEM and XRD pattern of the films. The SEM image for **a** 4 % NH_3 vapor, **b** 6 % NH_3 vapor, and **c** 8 % NH_3 vapor. The XRD pattern of the unheated film and annealed film at 500 °C for 2 h using 32 µM concentration of PVA and 6 % NH_3 vapor is shown in **d**

vapor in the reaction chamber can be observed. The films obtained for 4 and 6 % vapors of NH_3 are composed of nanoparticles having diameters of about 10 nm (Fig. 3a, b). The film obtained for 8 % of NH_3 vapor, although possesses nanoparticles having a diameter of about 10 nm, has nanoparticles in the aggregated form as shown in the inset of Fig. 3c. Therefore, due to the increase in concentration of NH_3 vapor, aggregation of the nanoparticles takes place which causes surface roughness of the films, but there is no change in the phase and composition of the films on varying the NH_3 concentration. The root mean square (rms) surface roughness of these films was measured by AFM. Other than the surface roughness caused by the variation in the percentage of NH_3 vapor, some small cracks are also observed. These cracks are either thermal-induced cracks (Glasscock et al. 2008) or have been produced by the stress induced during the transfer of the films from the surface of the liquid to the surface of the substrate as observed in the SEM images (Fig. 3a, b). For the film formed at moderate concentration viz. 6 % of NH_3 vapor concentration, XRD characterizations were used. The XRD pattern shown in Fig. 3d corresponds to the heated and unheated films formed at 6 % of NH_3. In the XRD pattern, the annealed sample contains the peaks at 2θ (32.3 and 35.4). These peaks are in accordance with the Joint Committee on Powder Diffraction Standards [JCPDS, file no. 89-8104] and correspond to α-Fe_2O_3. The particle size has also been calculated using the Scherrer formula $d = 0.94\lambda/\beta \cos\theta$, where λ is the wavelength of the X-ray used. The calculated particle size of 20 nm is close to the particle diameter observed in the SEM image.

For the TEM characterization, the films formed on the surface of the solution were transferred directly on a carbon-coated TEM copper grid. Figure 4a shows a TEM image of the film formed for 4 % vapor of NH_3 and annealed at 500 °C for 2 h. Here, almost a uniform size of the α-Fe_2O_3 nanoparticles ranging from 10 to 15 nm can be observed. There is a small clustering of the nanoparticles and the film possesses a uniform distribution of α-Fe_2O_3 nanoparticles. Further, the film was characterized by AFM for surface morphology and roughness.

Figures 4b, c are the AFM images of the film obtained for 4 % NH_3 vapor. The root mean square (rms) roughness is 1.34 nm as obtained from the AFM analysis.

For 6 % NH_3 vapor, although the diameter of nanoparticles remains between 10 and 15 nm, their aggregation starts as shown in the TEM image in Fig. 5a. The aggregation is also observed in the AFM image as shown in Fig. 5b. In this case, the roughness of the film increases to 4.5 nm as measured using the AFM data of Fig. 5c.

For 8 % NH_3 vapor, the aggregation of nanoparticles increases further as shown in Fig. 6a–c and the whole film becomes thicker. By closely inspecting the images, the size of the nanoparticles inside the aggregate is found to be almost 10 nm. Also, the dark region in the TEM image (Fig. 6a) indicates the thickness of the film. Again, the roughness of the film also increases to 6.8 nm as observed in AFM measurements. Therefore, at higher percentages of the NH_3 vapor, the thickness of the film increases. The increase in the thickness of the film is due to the formation of a large number of nanoparticles on the surface of the solution for higher NH_3 percentages. A higher percentage of NH_3 vapor makes more NH_3 molecules available at the surface of the solution and changes the pH value at the surface rapidly, resulting in a relatively larger co-precipitation on the surface. The overall effect of a higher concentration of NH_3 is the formation of a thick film on the liquid–vapor interface.

Effect of PVA concentration

In the second case, the experiment was carried out using 16, 32, and 64 µM concentrations of PVA in the precursor solution. For the 16 µM concentration, the size of the nanoparticles composing the film is about 25 nm as shown in Fig. 7a. When we increased the PVA concentration to 32 µM, the size of the nanoparticles reduced to 10 nm as shown in Fig. 7b. On further increasing the PVA concentration to 64 µM, aggregated nanoparticles are observed. The possible reason that leads to the reduction in the size of nanoparticles with an increase of PVA is the capping effect of PVA. The increased concentration of PVA caps the surface of nanoparticles, which prevents their growth due to polymeric stabilization. For a PVA concentration of 64 µM, the particles are in the cluster form as shown in the SEM image (Fig. 7c) where the cluster is formed by the clustering of the small nanoparticles. Thus, the big particles are formed by the aggregation of the small nanoparticles. Therefore,

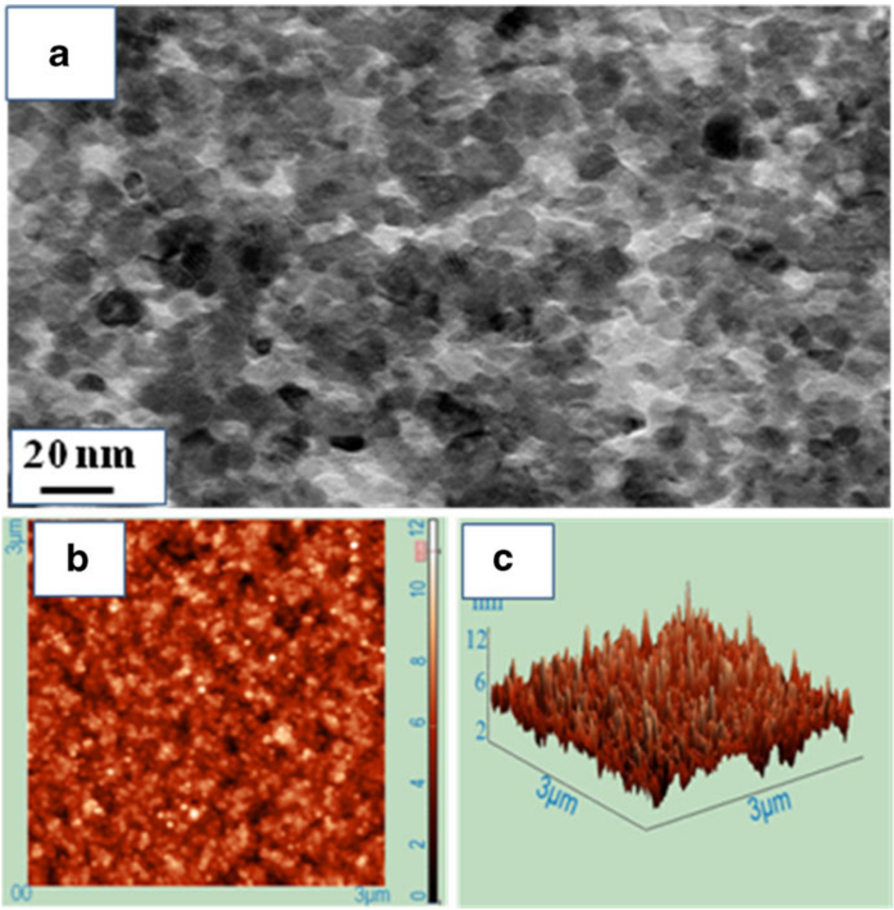

Fig. 4 **a** TEM image of the film formed for 4 % NH_3 vapor and 32 μM concentration of PVA, **b** AFM amplitude image, and **c** three-dimensional AFM image of the film

it can be stated that the aggregation of the nanoparticles starts as the concentration of PVA reaches 64 μM in the precursor solution. Due to the small size of the nanoparticles formed for the PVA concentration of 64 μM, the particles have higher surface energy. As soon as the temperature is increased to 500 °C, the PVA evaporates and the small nanoparticles aggregate to reduce their surface energy. So, the particles are observed in the aggregated form for higher concentrations of PVA.

Figure 7d shows the XRD spectrum of films formed for 16, 32, and 64 μM concentrations of PVA. In the XRD pattern, only two peaks at $2\theta = 33.2°$ and 35.9° are observed that correspond to α-Fe_2O_3. Therefore, from the XRD pattern, it can be concluded that with the change of PVA concentration, there is no change in the phase of the film contrary to the reported study (Uekawa and Kaneko 1998) in which they observed a change in phase probably due to the large concentration of PVA. In this study, in the XRD pattern, only the intensity of the peaks changes due to the change in the size of particles; smaller nanoparticles are formed inside the film for large concentrations of PVA. The particle size is calculated using the Scherrer formula; the lattice constants corresponding to the PVA concentrations are given in Table 1. The α-Fe_2O_3 exhibits a rhombohedral corundum structure and the corresponding lattice constant values are in agreement with the reported data (Sahoo et al. 2010).

Effect of annealing temperature

The films in this study were formed using a moderate concentration of PVA viz. 32 μM in the precursor solution. Figure 8a shows a TEM image of the unheated film, which is an amorphous structure. Also,

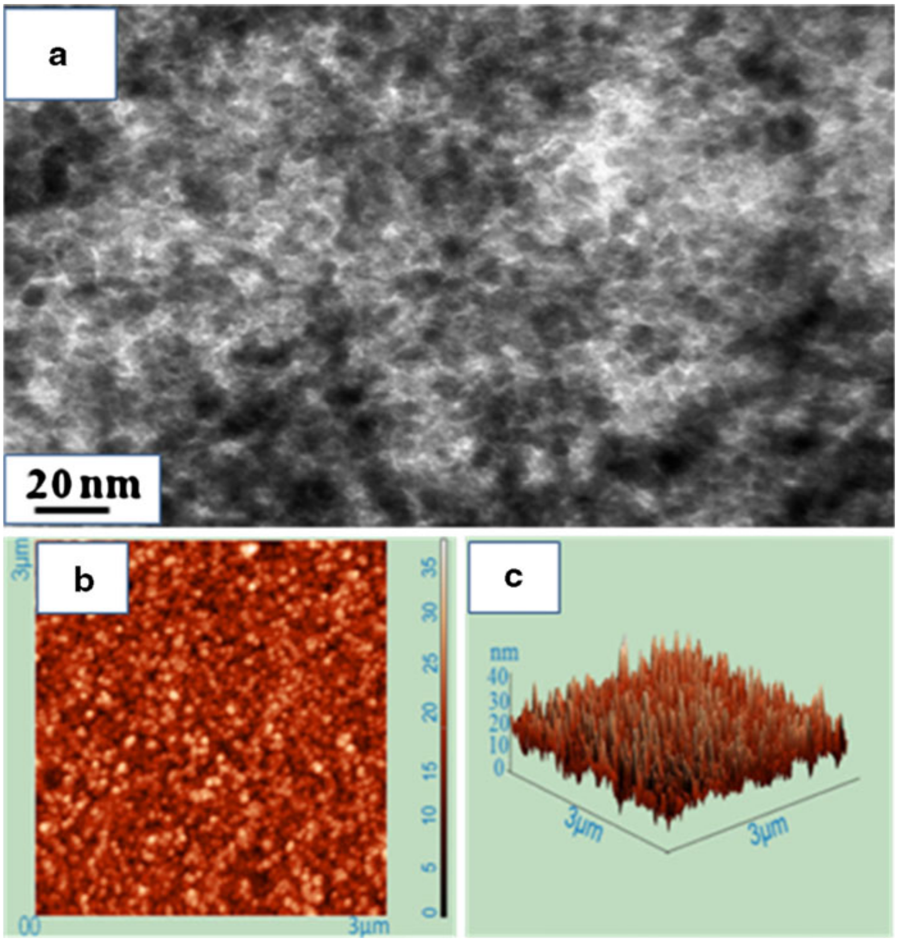

Fig. 5 **a** TEM image of the film formed for 6 % NH_3 vapor and 32 μM concentration of PVA, **b** AFM amplitude image, and **c** three-dimensional AFM image of the film

in the corresponding XRD pattern shown in Fig. 8f, no crystalline peak is observed, which confirms the amorphous nature of the film. For the film annealed at 250 °C, no peak is observed due to the amorphous nature of the film. For elemental composition, EDX analysis has been done during TEM analysis. The EDX spectrum of unheated film is shown in Fig. 8d. In the EDX analysis, the elements Fe and O are found to be in the atomic ratio 37.20:50.72 which corresponds to Fe_3O_4. To observe the effect of annealing temperature, the films were annealed for 2 h at 250 and 500 °C. The annealing of the films was carried out in a horizontal tube furnace in an Ar gas environment.

Figure 8b represents a TEM image of the film annealed at 250 °C for 2 h. In this film, nanoparticles of diameter <5 nm can be observed. Through the XRD study, we find that the crystalline nanoparticles are formed inside films that are annealed above 250 °C. This may be due to the fact that when the film is heated at 250 °C, the PVA evaporates and the amorphous α-Fe_2O_3 starts to crystallize into small α-Fe_2O_3 nanoparticles. Further, the annealing temperature was increased to 500 °C. The TEM image shown in Fig. 8c is the resultant film formed after annealing at 500 °C for 2 h. Here, the film contains crystalline nanoparticles having an average diameter of about 10 nm. The crystalline nature has also been detected in XRD (Fig. 8f). This indicates that an increase in the annealing temperature increases the size of the α-Fe_2O_3 nanoparticles inside the film. While analyzing the film formed after annealing at 250 and 500 °C, using EDX, almost a similar elemental composition has been observed. Figure 8e shows the EDX spectrum of the film annealed at 500 °C. Here, the elements Fe and O are in the ratio 32.98:49.19, forming Fe_2O_3. Thus, by changing the annealing temperature, the size of the nanoparticles inside the film can be varied, which then directly alters the surface area for the adsorption and its

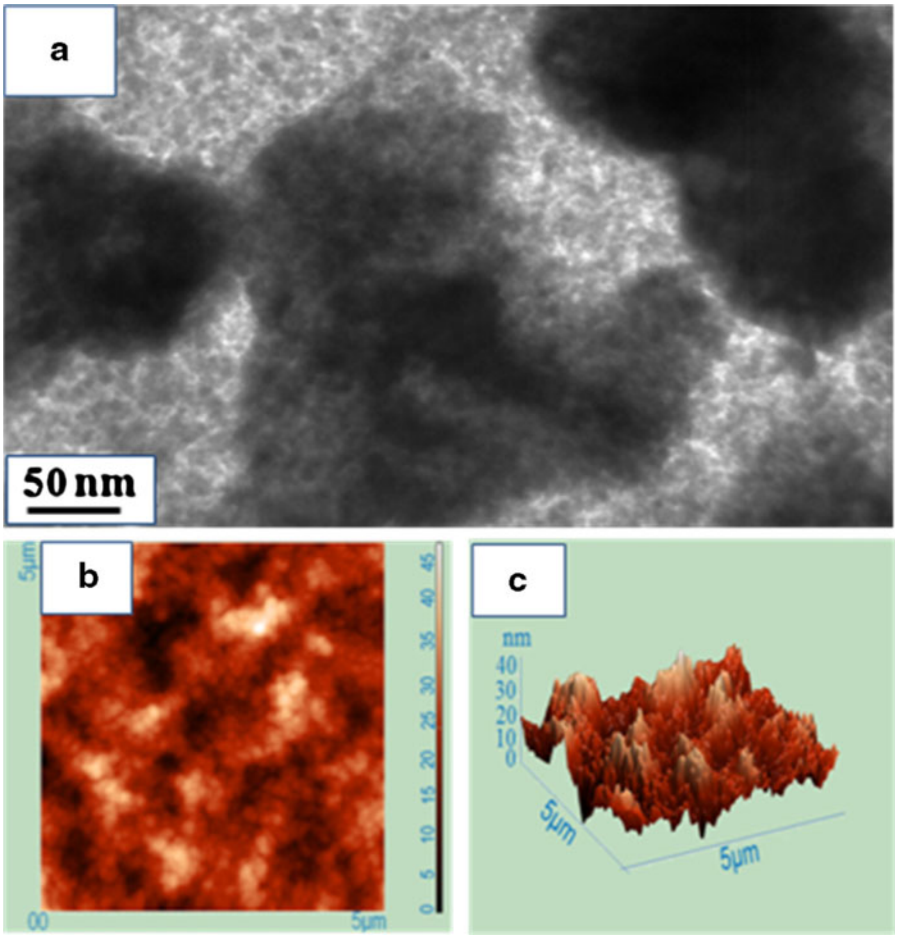

Fig. 6 **a** TEM image of the film formed for 8 % NH_3 vapor and 32 µM concentration of PVA, **b** AFM amplitude image, and **c** three-dimensional AFM image of the film

efficiency in applications of α-Fe_2O_3 films such as in solar cells, gas sensors, Li-ion batteries, and optical limiting can be improved.

Magnetic study

The α-Fe_2O_3 exhibits weak ferromagnetism above 260 K and antiferromagnetism below 260 K (Pastor et al. 2012). The transition temperature between antiferromagnetic and ferromagnetic is termed as the Morin transition (T_m) temperature. The observed weak ferromagnetism arises from the canting of the antiferromagnetically aligned spins above T_m. Nanoparticles of α-Fe_2O_3 phase also exhibit this behavior and the Morin temperature has been found to be strongly dependent on the size of the α-Fe_2O_3 particles; generally, it decreases with the decreasing size of the nanoparticles and it tends to disappear below a diameter of ~8 nm for spherical particles (Mansilla et al. 2002), even for 32 nm α-Fe_2O_3 nanoparticles for which a suppression of Morin temperature has been reported (Bhowmik and Saravanan 2010).

Field-cooled (FC) and zero field-cooled (ZFC) studies have been carried out by applying a magnetic field of $H = 100$ Oe to observe the effect of temperature on magnetization of the films that were annealed at 100, 250, and 500 °C temperatures; the magnetization versus temperature (M–T) plots are shown in Fig. 9a–c. In the M–T plots, a continuous increase in the magnetization of the films with decreasing temperature is observed, indicating suppression of the Morin transition. The increase in the magnetization with the decrease of temperature suggests an increase in superparamagnetic/paramagnetic contribution of uncompensated surface spin in antiferromagnetic grains (Bhowmik et al. 2004). Therefore, although the particle size increases with the annealing temperature, the size of nanoparticles is too small to

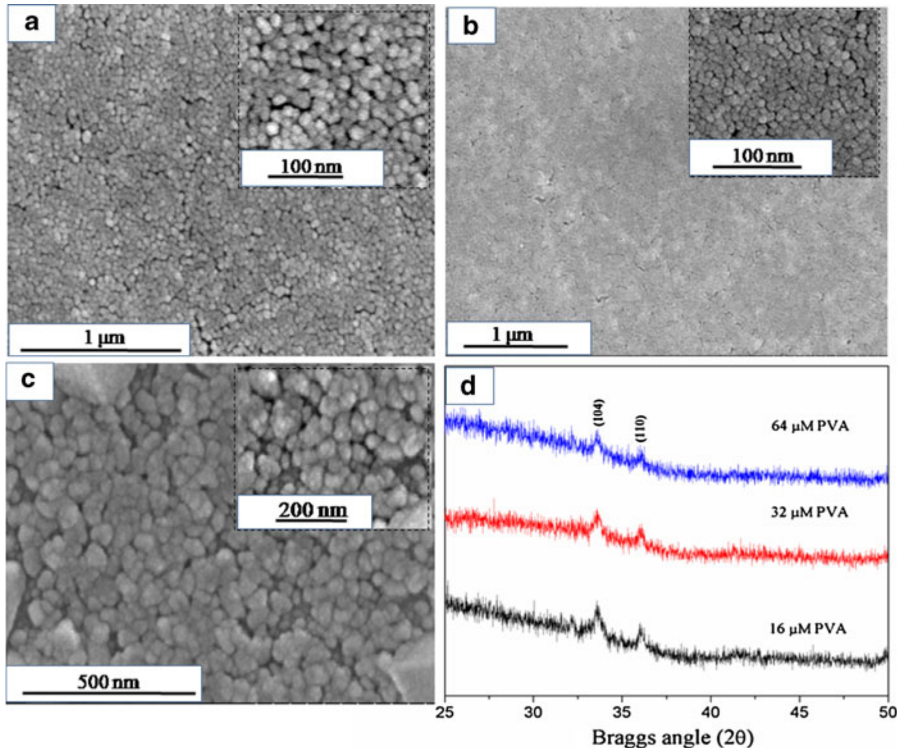

Fig. 7 SEM image of the films formed for **a** 16 μM, **b** 32 μM, and **c** 64 μM of PVA concentration at 6 % NH_3 vapor. **d** XRD patterns of the film for different PVA concentrations

Table 1 Calculated particle size and lattice parameter *a*, *b*, and *c* from the XRD data for film formed for 16, 32, and 64 μM concentrations of PVA

PVA concentration (μM)	*d* (nm) from XRD data	$a = b$ (Å)	*c* (Å)
16	18.43435	4.97	13.55
32	12.56788	4.97	13.56
64	12.38128	4.98	13.53

observe the Morin transition (Mansilla et al. 2002) even for the film annealed at 500 °C. For the films annealed at temperatures of 100, 250, and 500 °C, the M–H measurement at room temperature was also carried out using the VSM technique. The samples annealed at 100, 250, and 500 °C show a superparamagnetic behavior as shown in Fig. 9d. For these samples, the saturation magnetizations are 30.71, 35.17, and 42.78 emu/cm^3.

The observed saturation magnetization of 30.71, 35.17, and 42.78 emu/cm^3 for the α-Fe_2O_3 films annealed at 100, 250, and 500 °C temperatures, respectively, is much higher than that of the bulk value ($\sim$1 emu/cm^3) of α-Fe_2O_3. Although, in XRD, no peak was detected corresponding to the gamma phase (γ-Fe_2O_3) formation, from the observed higher values of magnetization on the films, it is inferred that during the annealing, a ferromagnetic gamma phase (γ-Fe_2O_3) also forms within a small fraction inside the film. Since the γ-Fe_2O_3 has a higher magnetic moment (430 emu/cm^3) as compared to α-Fe_2O_3, a small fraction γ-Fe_2O_3 inside the film is enough to enhance its saturation magnetization. Using standard values of the magnetization (bulk values) of the two phases, i.e., 1 emu/cm^3 for α-Fe_2O_3 and 430 emu/cm^3 for γ-Fe_2O_3, the concentration of the γ-Fe_2O_3 inside the film has been estimated using the formula $M_s = (x)(M \text{ of } \alpha\text{-}Fe_2O_3) + (1-x)(M \text{ of } \gamma\text{-}Fe_2O_3)$. Here, M_s is the observed total magnetization of the sample. We obtained 7.5, 8.2, and 10 % of γ-Fe_2O_3 phase ($1-x = 0.075$, 0.082, and 0.01) in the film annealed at temperatures of 100, 250, and 500 °C, respectively, alongside the remaining alpha phase nanoparticles. It may be noted here that the percentage of γ-Fe_2O_3 phase has been calculated using the bulk values of magnetization; however, in antiferromagnetic nanoparticles, the saturation magnetization could be higher than their bulk values due to the canting and uncompensated surface spins. Therefore, while considering the canting and uncompensated surface

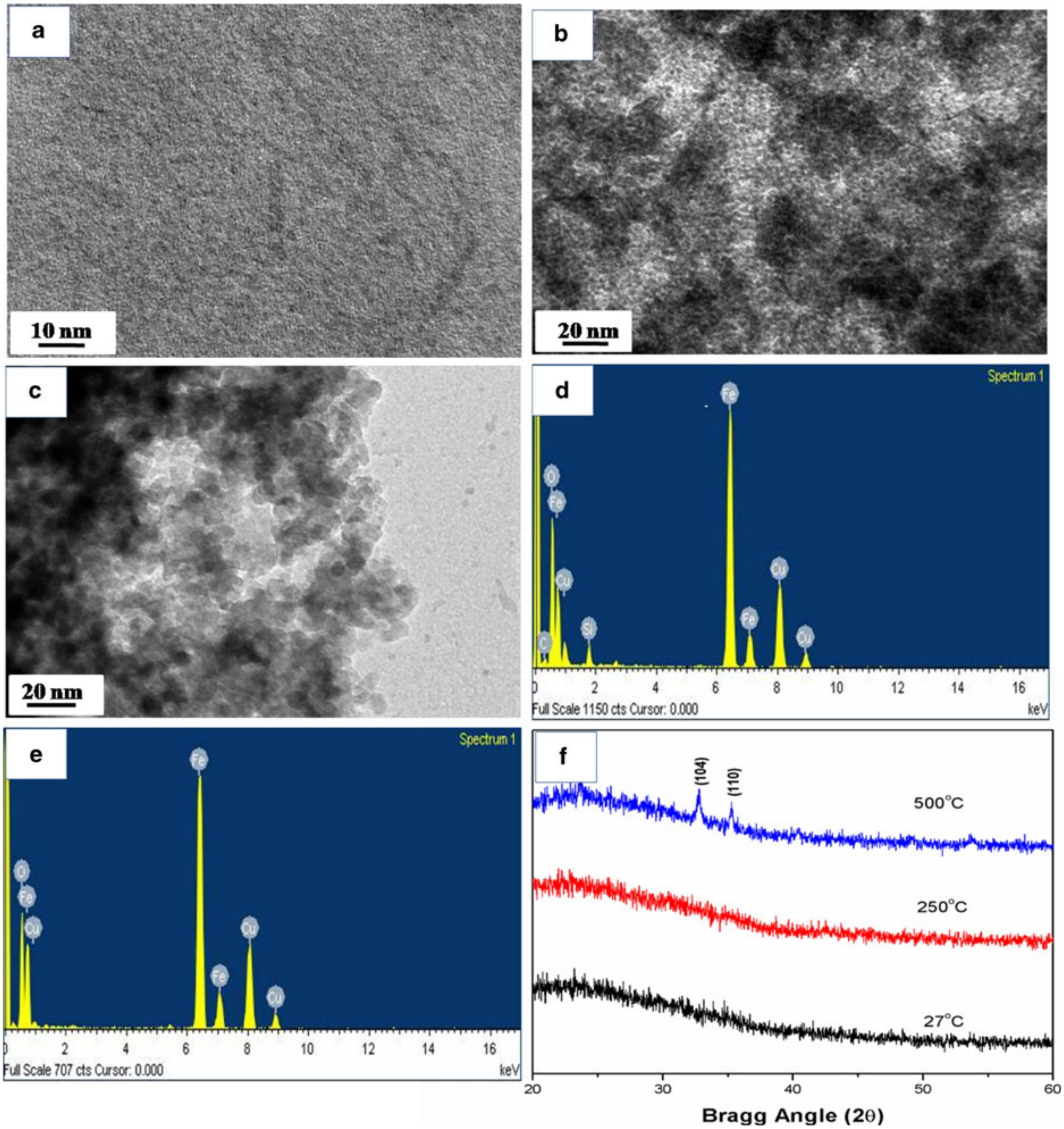

Fig. 8 **a–c** TEM images of unheated and annealed films at 250 and 500 °C temperatures. **d** EDX of the unheated film and **e** EDX of the film annealed at 500 °C temperature. **f** the XRD pattern of the unheated film and films annealed at temperatures of 250 and 500 °C for 2 h. All the films have been formed for 32 μM PVA concentration at 6 % of NH_3 vapor

spins, the percentage of γ-Fe_2O_3 phase would reduce correspondingly.

The observed room temperature superparamagnetic behavior of the films follows the Langevin function $M(H/T) = M_0$ [coth $(M_0mH/k_BT) - k_BT/M_0mH)$], (Parvin et al. 2004) as shown in Fig. 10, where M_0 is the saturation magnetization and m is the mass in grams of the individual particle. Taking the density of the material to be 5.2 g/cm^3, from the Langevin fit curves for the films annealed at 100, 250, and 500 °C, the calculated values of M_0 are 33.5, 36.8, and 44.0 emu/cm^3, respectively, which are in agreement with the values observed by the VSM technique.

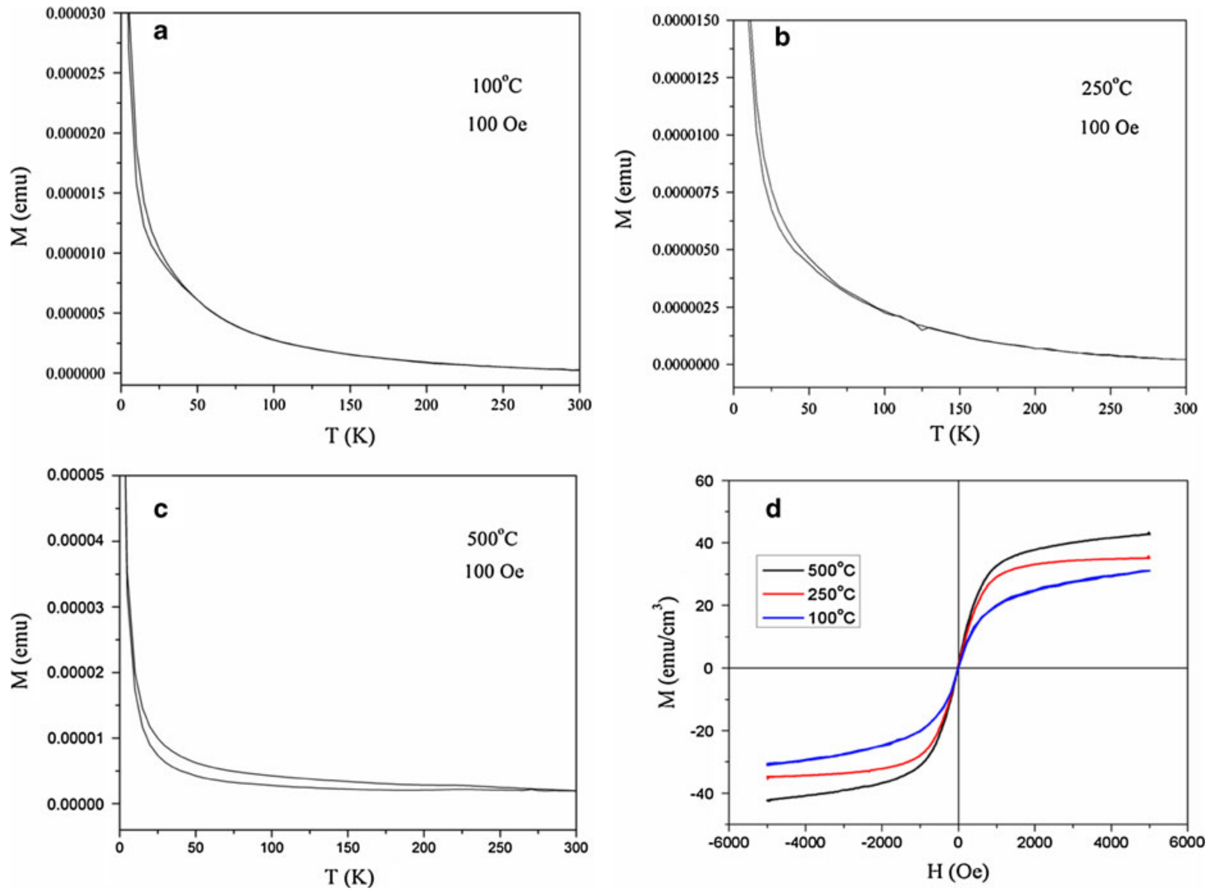

Fig. 9 M–T plot of the α-Fe_2O_3 films annealed at **a** 100 °C, **b** 250 °C, and **c** 500 °C temperatures. **d** M–H plot of these films at room temperature

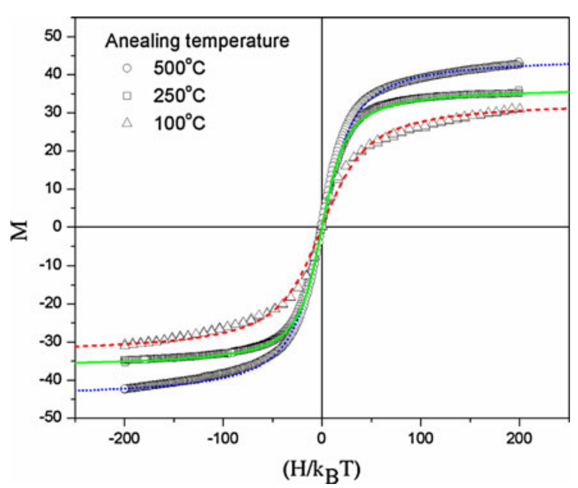

Fig. 10 M versus H/k_BT for films annealed at temperatures of 100, 250, and 500 °C with fitted Langevin function

Conclusions

In conclusion, the vapors of NH_3, PVA concentration, and annealing temperature have been found to play important roles in surface morphology/size of nanoparticles of the film. The roughness of the film surface increases with the increase of exposure to NH_3 vapor due to the aggregation of the nanoparticles. The size of the α-Fe_2O_3 nanoparticles inside the films can also be controlled by varying the annealing temperature and concentration of PVA inside the solution; this has many valuable applications such as in solar cells, Li-ion batteries, and gas sensors. The method presented here is a novel approach to control the thickness of the α-Fe_2O_3 film. The film formed on the solution surface can be transferred to any desired substrate. The films are superparamagnetic in nature.

Acknowledgments This study was partly supported by the National Research Foundation of Korea (NRF) Grant funded by the Korean government (MEST) (No. 2012-0005656) and by the Research Grant for Nanotechnology Lab, Jaypee University of Information Technology, Waknaghat, Solan (India).

References

Ahmmad B, Kusumoto Y, Abdulla-Al-Mamun M, Mihata A, Yang H (2009) Effect of single wall nanotubes as counter electrode on laser deposited Fe_2O_3 and TiO_2 films solar cells. J Sci Res 1:430–437

Aronniemi M, Lahtinen J, Hautojärvi P (2004) Characterization of iron oxide thin films. Surf Interface Anal 36:1004–1006

Aronniemi M, Saino J, Lathtinen J (2008) Characterization and gas sensing behavior of an iron oxide thin film prepared by atomic layer deposition. Thin Solid Films 516:6110–6115

Bhowmik RN, Saravanan A (2010) Surface magnetism, Morin transition and magnetic dynamics in antiferromagnetic α-Fe_2O_3 (hematite) nanograins. J Appl Phys 107:053916–053925

Bhowmik RN, Nagarajan R, Raganathan R (2004) Magnetic enhancement in antiferromagnetic nanoparticle $CoRh_2O_4$. Phys Rev B 69:054430–054435

Birkholz M, Lichtenberger D, Hfpfner C, Fiechter S (1992) Sputtering of thin pyrite films. Sol Energy Mater Sol Cells 27:243–251

Cesar I, Kay A, Martinez JAG, Gratzel M (2006) Translucent thin film Fe_2O_3 photo anodes for efficient water splitting by sun light: nanostructure-directed effect of Si doping. J Am Chem Soc 128:4582–4583

Chandra V, Park J, Chun Y, Lee JW, Hwang IC, Kim KS (2010) Water-dispersible magnetite-reduced graphene oxide composites for arsenic removal. ACS Nano 4:3979–3986

Chatzitheodorou G, Fiechter S, Kfnenkamp R, Kunst M, Jaegermann W, Tributschthin H (1986) Photo active FeS_2 (pyrite) films. Mater Res Bull 21:1481–1487

Chirita M, Grozescu I (2009) Fe_2O_3-nanoparticle, physical properties and their photochemical and photoelectrochemical application. Chem Bull "POLITEHNICA" Univ (Timisoara) 54:1–8

Dong Q, Yin S, Guo CS, Li HH, Kumada N, Takei T, Yonesaki Y, Kinomura N, Sato T (2012) Preparation of α-Fe_2O_3 particles with controlled shape and size via a facile hydrothermal route. JPCS 339:012004

Fu YY, Wang RM, Xu J, Chen J, Y Y, Narlikar AV, Zhang H (2003) Synthesis of large arrays of aligned α-Fe_2O_3 nanowires. Chem Phys Lett 379:373–379

Ge S, Shi XY, Sun K, Li CP, Uber C, Baker JR, Banaszak Holl MM Jr, Orr BG (2009) Facil hydrothermal synthesis of iron oxide nanoparticles with tunable magnetic properties. J Phys Chem C 113:13593–13599

Glasscock JA, Barnes PRF, Plumb IC, Savvides N (2007) Enhancement of photoelectrochemical hydrogen production from hematite thin films by the introduction of Ti and Si. J Phys Chem C 111:16477–16488

Glasscock JA, Barnes IC, Plumb IC, Bendavid A, Martin PJ (2008) Structural, optical and electrical properties of undoped polycrystalline hematite thin films produced using filtered arc deposition. Thin Solid Films 516:1716–1724

Gou X, Wang G, Park J, Liu H, Yang J (2008) Monodisperse hematite porous nanospheres: synthesis, characterization, and application for gas sensors. Nanotechnology 19:125606

Hwang IC, Kumar R, Kim ND, Chun Y, Lee JW, Kumar P, Mana RS, Choi C, Lee JR, Kim KS (2009) Controlling metal nanotoppings on the tip of silicide nanostructure. Nanotechnology 20:245605

Jia CJ, Sun LD, Yan ZG, You LP, Luo F, Han XD, Pang YC, Zhang Z, Yan CH (2005) Single crystalline iron oxide nanotubes. Angew Chem Int Ed 44:4328–4333

Jin YH, Deok S, Shim HW, Park KS, Kim DW (2012) Synthesis of core/shell spinel ferrite/carbon nanoparticles with enhanced cycling stability for lithium ion battery anodes. Nanotechnology 23:125402

Kay A, Cesar I, Gratzel M (2006) New benchmark for water photooxidation by nanostructured α-Fe_2O_3 films. J Am Chem Soc 128:15714–15721

Kim JY, Jun H, Hong SJ, Kim HG, Lee JS (2011) Charge transfer in iron oxide photoanode modified with carbon nanotubes for photoelectrochemical water oxidation: an electrochemical impedance study. Int J Hydrogen Energ 36:9462–9468

Kumar R, Gautam S, Hwang IC, Lee JR, Chae KH, Thakur N (2009) Preparation and characterization of α-Fe_2O_3 polyhedral nanocrystals via annealing technique. Matter Lett 63:1047–1050

Lin H, Watanabe Y, Kimura M, Hanabusa K, Shirai H (2003) Preparation of magnetic polyvinyl alcohol (PVA) materials by in situ synthesis of magnetite in a PVA matrix. J Appl Polym Sci 87:1239–1247

Lindgren T, Wang H, Beermann N, Vayssieres L, Hagfeldt A, Lindquist SE (2002) Aqueous photoelectrochemistry of hematite nanorod arrays. Sol Energy Mater Sol Cells 71:231–243

Liu Z, Sha J, Yang Q, Su Z, Zhang H, Yang D (2007a) Flower-like silicon nanostructures. Phys E 38:27–30

Liu ZL, Liu CC, Yao KL, Liu PD, Ning Q (2007b) Preparation and characterization of micron-sized magnetic microspheres by one-step suspension polymerization. J Appl Polym Sci 105:1331–1335

Mahapatra SK, John SE, Banerjee S, Mishra M (2009) Water photooxidation by smooth and ultrathin α-Fe_2O_3 nanotubes arrays. Chem Mater 21:3048–3055

Mansilla MV, Zysler R, Fiorani D, Suber L (2002) Annealing effect on magnetic properties of acicular hematite nanoparticles. Phys B 320:206–209

Mathur S, Sivakov V, Shen H, Barth S, Cavelius C, Nilsson A, Kuhn P (2006) Nanostructured film of iron, tin and titanium oxide by chemical vapor deposition. Thin Solid Films 502: 88–93

Miller EL, Paluselli D, Marsen B, Rocheleau RE (2004) Low temperature reactivity sputtered iron oxide for thin film devices. Thin Solid Films 466:307–313

Morishita N, Malagami H, Morishita R, Takeda S, Mishima F, Terazono B, Nishijima S, Kaneda Y, Tanaka N (2005) Magnetic nanoparticles with surface modification enhanced gene delivery of HVJ-E vector. Biochem Biophys Res Commun 334:1121–1126

Mulmudi HK, Mathews N, Dou XC, Xi LF, Pramana SS, Lam YM, Mhuisalkar SG (2011) Controlled growth of hematite (α-Fe_2O_3) nanorod array on flourin doped tin oxide: synthesis and photoelectrochemical properties. Electrochem Commun 13:951–954

Omi S, Kanetaka A, Shimamori Y, Supsakulchai A, Nagai M, Ma GH (2001) Magnetite (Fe_3O_4) microcapsules prepared using a glass membrane and solvent removal. J Microencapsul 18:749–765

Park CD, Walker J, Tannenbaum R, Stiegman AE, Frydrych J, Machala L (2009) Sol-gel derived iron oxide thin films on silicon: surface properties and interfacial chemistry. ACS Appl Mater Interfaces 1:1843–1846

Parvin K, Ma J, Ly J, Sun XC, Nikles DE, Sun K, Wang LM (2004) Synthesis and magnetic properties of monodisperse Fe_3O_4 nanoparticles. J Appl Phys 95:7121–7123

Pastor JM, Pérez-Landazalol JI, Gómez-Polo C, Recarte V, Larumbe S, Santamarta R, Silva MF, Pineda EAG, Hechenleitner AAW, Lima MK (2012) Entropy change linked to the magnetic field induced Morin transition in hematite nanoparticles. Appl Phys Lett 100:063102

Ramachandran B, Ramachandra Rao MS (2007) Optical and magnetic properties of monodispersed α–Fe_2O_3 nanoparticle aggregates. AIP Conf Proc 1003:91–93

Ryu HS, Kim JS, Guo Z, Liu H, Kim KW, Ahn JH, Ahn HJ (2010) Electrochemical properties of Fe_2O_3 thin film fabricated by electrostatic spray deposition for lithium-ion batteries. Phys Scr T139:014066

Sahoo SK, Agarwal K, Singh AK, Polke BG, Raha KC (2010) Characterization of γ- and α-Fe_2O_3 nanopowder synthesized by emulsion precipitation–calcination rout and rheological behavior of α-Fe_2O_3. IJEST 8:118–126

Shen S, Kronawitter CX, Jiang J, Mao SS, Guo L (2012) Surface tuning for promoted charge transfer in hematite nanorod arrays as water-splitting photoanodes. Nano Res 5:327–336

Shinde SS, Bansode RA, Bhosale CH, Rajpure KY (2011) Physical properties of hematite α-Fe_2O_3 thin films: application to photo electrochemical solar cells. J Semicond 32:013001–013008

Singh CP, Bindra KS, Bhalera GM, Oak SM (2008) Investigation of optical limiting in iron oxide nanoparticles. Opt Express 16:8440–8450

Sivako V, Petersen C, Daniel C, Shen H, Mucklich F, Mathur S (2005) Laser induced local and periodic phase transformations in iron oxide thin films obtained by chemical vapour deposition. Appl Surf Sci 247:513–517

Turkovoć A, Ivanda M, Bitenc M, Orel ZC (2011) Influence of Lithium on nanosized film of Fe_2O_3. J Nanomater 967307:1–8

Uekawa N, Kaneko N (1998) Nonstoichiometric properties of nanoporous iron oxide films. J Phys Chem B 102:8719–8724

Wu C, Yin P, Zhu X, Yang CO, Xie Y (2006) Synthesis of hematite (α-Fe_2O_3) nanorods; diameter size and shape effect on their application in magnetism, lithium ion battery and gas sensors. J Phys Chem B 110:17806–17812

Zang Z, Hossain MF, Miyazaki T, Takahashi T (2010) Gas phase photocatalytic activity of ultrathin Pt layer coated on α-Fe_2O_3 films under visible light illumination. Environ Sci Technol 44:4741–4746

Zhang J, Liu X, Wang L, Yang T, Guo X, Wu S, Wang S, Zhang S (2011) Synthesis and gas sensing properties of α-Fe_2O_3@ZnO core–shell nanospindles. Nanotechnology 22:185501

Zhou HS, Mito A, Kundu D, Honma I (2000) Nonlinear optical susceptibility of Fe_2O_3 thin film synthesized by a modified sol-gel method. J Sol-Gel Sci Technol 19:539–541